Limited Mitigation Potential of Forestation Under a High Emissions Scenario: Results From Multi-Model and Single Model Ensembles

Tammas F. Loughran[1] [ID]**, Tilo Ziehn[1]** [ID]**, Rachel Law[1]** [ID]**, Josep G. Canadell[2]** [ID]**, Julia Pongratz[3,4]** [ID]**, Spencer Liddicoat[5]** [ID]**, Tomohiro Hajima[6]** [ID]**, Akihiko Ito[7]** [ID]**, David M. Lawrence[8]** [ID]**, and Vivek K. Arora[9]** [ID]

[1]CSIRO Environment, Aspendale, VIC, Australia, [2]CSIRO Environment, Canberra, ACT, Australia, [3]Ludwig-Maximilians-Universität München, Munich, Germany, [4]Max Planck Institute for Meteorology, Hamburg, Germany, [5]Met Office Hadley Centre, Exeter, UK, [6]Research Institute for Global Change, Japan Agency for Marine-Earth Science and Technology, Kanagawa, Japan, [7]National Institute for Environmental Studies, Tsukuba, Japan, [8]Climate and Global Dynamics Laboratory, National Center for Atmospheric Research, Boulder, CO, USA, [9]Canadian Centre for Climate Modelling and Analysis, Environment and Climate Change Canada, University of Victoria, Victoria, BC, Canada

Abstract Forestation is a major component of future long-term emissions reduction and CO_2 removal strategies, but the viability of carbon stored in vegetation under future climates is highly uncertain. We analyze the results from seven CMIP6 models for a combined scenario with high fossil fuel emissions (from SSP5-8.5) and forest expansion (from SSP1-2.6) which has ∼4.8% increase in global total forest cover relative to 2015. This scenario aims to demonstrate the ability of forestation strategies to mitigate climate change under continued increasing CO_2 emissions and includes the potential impacts of increased CO_2 concentration and a warming climate on vegetation growth. The model intercomparison shows that forestation as a CO_2 removal strategy has limited impact on global climate under a high global warming scenario, despite generating a substantial cumulative carbon sink of 10–60 Pg C over the period 2015–2100. Using a single model ensemble, we show that there are local increases in warm extremes in response to forestation associated with decreases in the number of cool days. Furthermore, we find evidence of a shift in the global carbon balance, whereby increased carbon storage on land of ∼25 Pg C by 2100 associated with forestation has a concomitant decrease in the carbon uptake by the ocean due to reduced atmospheric CO_2 concentrations.

Plain Language Summary We use seven model projections to estimate future climates in which forestation occurs under a high fossil fuel emission scenario. While the forestation in this scenario is not enough to substantially mitigate global warming, the new forest cover makes up a stable carbon sink over the next century.

1. Introduction

Forests cover approximately 31% of the global land surface (FAO, 2020; Luyssaert et al., 2014) and the terrestrial biosphere is currently responsible for the removal of 30% of total anthropogenic emissions from the atmosphere (Friedlingstein et al., 2022). Forestation is therefore often thought of as a viable strategy to remove CO_2 from the atmosphere and mitigate global warming (Griscom et al., 2017; House et al., 2002; Smith et al., 2022). Most decarbonization pathways to limit global warming to below 1.5 or 2°C (consistent with the Paris Agreement) require not only a reduction of fossil fuel emissions, but also CO_2 removal to offset industrial and agricultural emissions that are difficult to abate (Babiker et al., 2022). The most commonly used practice to remove CO_2 from the atmosphere in decarbonization pathways is forestation that includes a) reforestation: forest regrowth in abandoned agricultural and pasture lands, and direct tree planting, and b) afforestation: tree planting in areas not previously forested.

Forestation and deforestation affect the climate in two main ways (Ito & Hajima, 2020; Pongratz et al., 2010; Zhu et al., 2023). Firstly, by biogeochemical effects, that is, changes to the global carbon cycle and carbon storage pools that affect atmospheric CO_2 concentration and, therefore, the radiative absorption of the atmosphere. And secondly by biogeophysical effects, that is, changes in the physical properties of the land surface such as albedo, roughness and evapotranspiration efficiency, which in turn influence the surface energy balance (Bala

et al., 2007; Betts, 2000; Winckler et al., 2019). In general, forestation causes a global cooling biogeochemical effect as carbon is taken from the atmosphere and stored in vegetation and soils. However, the biogeophysical impacts of forestation are more varied, with the effects of albedo and roughness having opposing impacts that might dominate more or less at different latitudes.

Historically, there has been substantial deforestation in temperate forests of Eurasia and North America and in the last few decades, deforestation has been focused on the tropics (Klein Goldewijk, 2001). The net effect of deforestation is to cool the climate globally due to an increase in albedo (Davin & de Noblet-Ducoudré, 2010). While the albedo-induced cooling is a result of the changes in the global planetary energy balance, reinforced by the ocean, the biogeophysical effects at the site of the deforestation are generally a warming effect (Betts, 2001; Kumar et al., 2013; Lee et al., 2011; Li et al., 2016; Winckler, Lejeune, et al., 2019): Locally, the reduction in absorbed energy is compensated for by a reduction in turbulent heat fluxes (Winckler et al., 2019). As a result, the albedo changes have a minor influence on local temperatures. Instead, the reduction in roughness transforming forest to short, smooth grass or cropland vegetation leads to less efficient transfer of heat from the surface into the atmosphere, which induces warming both in the annual mean and daily and seasonal warm extremes (Winckler, Reick, Luyssaert, et al., 2019). The amount of CO_2 removed from the atmosphere and the climate impacts can be simulated with earth system model projections. The land surface components of these models simulate vegetation dynamics to varying degrees and their interaction with the atmosphere can estimate a range of possible carbon cycle and climate impacts (for a recent overview on the current state of land surface modeling dynamics see Fisher et al. (2018) and Argles et al. (2022)).

Model results are confirmed by observation-based estimates (which by way of their setup capture only local effects; Alkama and Cescatti (2016); Bright et al. (2017) and see Pongratz et al. (2021) for a review of the climatic effects of forest cover changes from local to global scale). In another modeling study of deforestation, Boysen et al. (2020) show a cooling of $-0.22 \pm 0.2°C$ among nine climate models in idealized deforestation simulations with constant atmospheric CO_2 concentration; in the tropics, the warming effect of local surface property changes dominates over the global cooling signal in most models. Hong et al. (2022) also show that under a future deforestation scenario, this cooling effect might reduce the incidence of hot extremes by 0.9%–5.5%. However, the effect of future forestation may not necessarily be merely the inverse of the effect of future deforestation.

There have been several previous studies on the potential of forestation to remove CO_2 from the atmosphere, each using different methods of quantification. For example, early studies like House et al. (2002) approximated the maximum hypothetical potential change in CO_2 concentration (40–70 ppm by 2100) due to reversing all historical forest losses. Similarly, Lenton and Vaughan (2009) used a simplified "back-of-the-envelope" analytical calculation approach to estimate the radiative forcing effect of forestation, finding that it has substantial potential relative to most other geoengineering methods. They estimate a removal of 73 Pg C by forestation can result in a decrease of 0.37 W m^{-2} radiative forcing by 2100. However, besides assuming hypothetical scenarios of forestation, such simplified estimates largely disregard impacts of future environmental changes on forests and assume that the land carbon storage is stable on long time scales, the decay of which under a future climate could only be estimated with an earth system model.

More sophisticated modeling studies better represent the complexity of the net effects of biogeophysical and biogeochemical impacts and their dynamics depending on future environmental changes. For example, Sonntag et al. (2016) quantified the CO_2 removal potential using an Earth System Model, in which a high CO_2 emissions scenario is simulated (taken from RCP8.5) in combination with the "forestation" land-use from a low emissions scenario (taken from RCP4.5). This study used the concentration-driven CMIP5 (Coupled Model Intercomparison Project Phase 5) version of the MPI-ESM and the CMIP5 representative concentration pathways. They find that a decrease of about 85 ppm (215 Pg C) in atmospheric CO_2 concentrations by 2100 from forestation results in a cooling of 0.27 K globally, with a dampening of heat extremes through biogeophysical effects in some densely populated regions (also reiterated in Sonntag et al. (2018)).

Some other experimental designs kept to idealized assumptions and represented a more extreme deployment of forestation, where a large and potentially unfeasible portion of non-forested lands are forested. De Hertog et al. (2022), for example, conducted an experiment where all non-forested lands, except bare ground, are forested in a checker-board pattern. While this is not meant as a real-world application, it allows for the diagnosis of local and non-local effects of forestation, demonstrating that in those models the local biogeophysical effects from forestation produce a cooling in the tropics, while the non-local effects result in a large-scale warming.

To date, a multi-model intercomparison of the potential of forestation to store CO_2 and mitigate climate change under a realistic scenario is lacking from the literature (while Ito et al. (2020) examined soil carbon, they did not examine the entire terrestrial biosphere or the climate impacts). This study aims to quantify the CO_2 removal potential of forestation in a high-emissions scenario (SSP5-8.5) using CMIP6 models in an interactive emissions-driven carbon cycle configuration. We will assess the viability of the carbon stores, and the net impacts of forestation on the climate. The CMIP6 ensemble of models provides a measure of uncertainty related to model structure and parameters. Furthermore, there is an ensemble of simulations available for a single model for the estimation of uncertainty arising from internal climate variability.

2. Methods

2.1. Experiments

The CMIP6 experimental design specifies a set of standard simulations called the Diagnostic, Evaluation and Characterization of Klima (DECK) (Eyring et al., 2016), which are typically used as the foundation to study more specific research questions. The DECK includes a pre-industrial control simulation (*piControl*) with constant greenhouse gas concentration forcing, and a historical (*historical*) simulation with transient historical greenhouse gas concentration forcing. Furthermore, the DECK specifies corresponding simulations (*esm-piControl* and *esm-hist*) that are run in "Earth system model" mode (i.e., with a fully interactive dynamic carbon cycle) wherein historical fossil fuel and industrial greenhouse gas emissions are used to force the models. Projection period emissions-driven simulations that are analyzed in this study were initialized at 2015 from the end of the *esm-hist* experiments.

The reference simulation we use to compare to the forestation scenario is the *esm-ssp585* from the Coupled Climate-Carbon Cycle Model Intercomparison Project (C4MIP) (Jones et al., 2016). This is the emissions-driven Earth system model simulation corresponding to the SSP5-8.5 high greenhouse gas scenario that assumes that development is driven by fossil fuels (O'Neill et al., 2016).

The forestation scenario analyzed here is the Land Use Model Intercomparison Project's *esm-ssp585-ssp126Lu*, spanning the years 2015–2100 (Lawrence et al., 2016). Compared to SSP5-8.5, this scenario has ∼4.8% increase in forest cover. This simulation features the surface fossil fuel-related CO_2 emissions from the SSP5-8.5 scenario, but the land-use trajectory is taken from the SSP1-2.6 scenario (O'Neill et al., 2016). The SSP5-8.5 scenario represents a high emissions future pathway that results in a radiative forcing of 8.5 W m^{-2} in 2100. The SSP1-2.6 scenario land-use change assumes a future of sustainable development (van Vuuren et al., 2017). This scenario assumes low population growth, low pressures on land-use, expansion of protected lands, environmentally friendly changes in diets and increased agricultural efficiency and yields, which altogether drive the abandonment of agricultural lands. This abandoned agricultural land allows for the expansion of natural lands and forest cover. We use this scenario because it represents a plausible future forestation scenario that would provide a lower bound on the survivability of vegetation and CO_2 removal potential of the land surface under a warmer climate.

In general, there is greater forest expansion occurring in *esm-ssp585-ssp126Lu* than *esm-ssp585*. By taking the difference between the forestation simulation and the *esm-ssp585* simulation for any variable X (Equation 1), we can examine the impact of forestation on the climate and the carbon cycle. Therefore, we use the term "forestation" to include the avoidance of deforestation that also occurs in SSP5-8.5.

$$X|_{for} = X|_{esm-ssp585-ssp126Lu} - X|_{esm-ssp585} \qquad (1)$$

The land-use change data used in all CMIP6 experiments are the Land-use Harmonization data set version 2 (LUH2; Hurtt et al., 2020), which for future scenarios is derived from integrated assessment models (IAMs). LUH2 provides land-use states and transitions as relatively generic types such as primary and secondary forested and non-forested land. These data are translated by each modeling group to changes in the fractional coverage of either specific plant functional types (PFTs) or more general land-use and land-cover types if PFT competition dynamics are simulated (e.g., Di Vittorio et al., 2014). Figure 1 shows the temporal change in combined primary and secondary forest cover fractions from LUH2 data. The SSP1-2.6 land-use change is typically characterized by forestation, while the SSP5-8.5 has a mixture of deforestation and forestation. SSP5-8.5 land-use change has no net change in global forest cover for most of the century with a small amount of forestation occurring in the last few decades, however, there is considerable deforestation in the central African region (Figure 1b). The difference in forest area between the two scenarios (Figure S1 in Supporting Information S1) is about 3 million km^2 (which
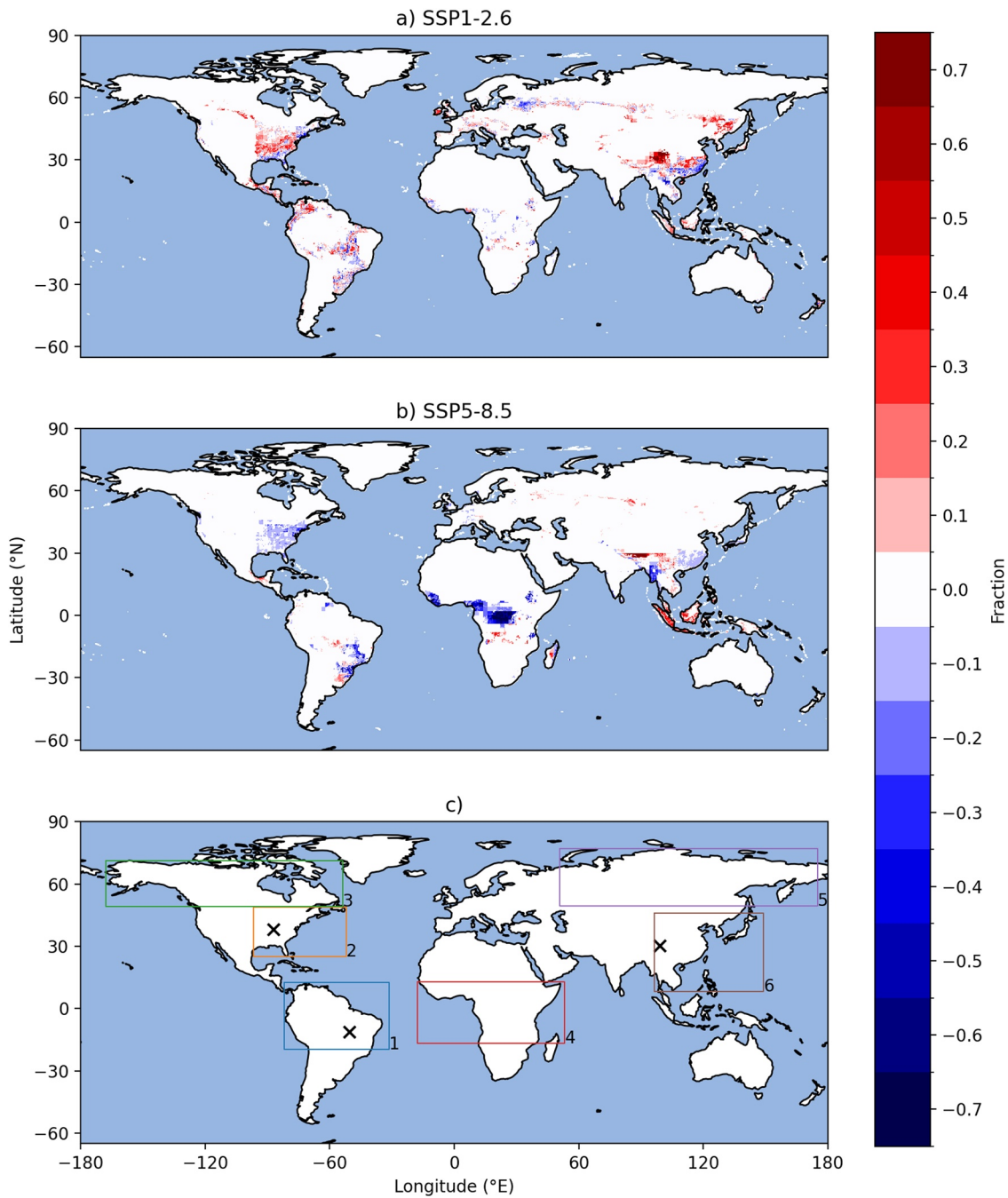
Figure 1. Temporal anomaly (2100 – 2015) in tree fraction from the Land-use Harmonization 2 for (a) the SSP1-2.6 scenario and (b) the SSP5-8.5 scenario between the year 2100 and 2015. (c) Boxes demark the areas used in the ACCESS-ESM1-5 regional analysis. The regions are 1 Amazonia, 2 Northeast North America, 3 Boreal North America, 4 Central Africa, 5 Boreal Eurasia, and 6 East Asia. The black crosses mark the locations of large forestation changes that are used for daily temperature distributions in Eastern North America (275°E, 37.5°N), East Asia (99.375°E, 32.5°N), and Amazonia (311.25°E, −12.5°N).

is an area about the size of India and ~4.8% increase in global total forest cover), about 50% of which is avoided deforestation in the SSP5-8.5 scenario. There are only a few small areas where there is deforestation in the SSP1-2.6 experiment. These occur in deciduous broad leaf forests in eastern North America, China and western Russia (Figure 1a). Furthermore, we acknowledge that the LUH2 SSP1-2.6 scenario underestimates the tree cover that was originally dictated by IMAGE (the IAM that produces the SSP1-2.6 scenario). This is due to differences in the definition of tree cover in the integrated assessment models as well as the effects of harmonization of that data with observed historical land cover fractions. LUH2 provided additional forest cover data to match the forestation

Table 1
Models Participating in Both Land-Use Model Intercomparison Project and Coupled Climate-Carbon Model Intercomparison Project With Available Simulations for esm-ssp585-ssp126Lu and esm-ssp585

Model	Fire	N	P	PFT dyn.	Demography	PFTs	Natural PFTs	Resolution	LSM reference	ESM reference
ACCESS-ESM1-5	No	Yes	Yes	No	No	10	9	$1.8758 \times 1.258°$	Kowalczyk et al. (2006); Wang et al. (2010); Harman et al. (2019)	Ziehn et al. (2020)
CanESM5	No	No	No	No	Yes	9	7	$2.8 \times 2.8°$	Verseghy (2000); Arora and Boer (2005)	Swart et al. (2019)
GFDL-ESM4	Yes	No	No	Yes	Yes	7	5	100×100 km	Zhao et al. (2018)	Dunne et al. (2020)
MIROC-ES2L	No	Yes	No	No	No	14	13	$2.8 \times 2.8°$	Ito and Inatomi (2012)	Hajima et al. (2020)
MPI-ESM1-2-LR	Yes	Yes	No	Yes	No	12	8	$1.8° \times 1.8°$	Reick et al. (2013)	Mauritsen et al. (2019)
CESM2	Yes	Yes	No	No	No	22	14	$1.25° \times 0.9°$	Lawrence et al. (2019)	Danabasoglu et al. (2020)
UKESM1-0-LL	No	Yes	No	Yes	Yes	12	9	$1.25 \times 1.875°$	Best et al. (2011); Burton et al. (2019)	Sellar et al. (2019)

Note. The columns indicate whether the model's land surface component has representations of wildfire, Nitrogen (N) and Phosphorus (P) cycles, plant functional types dynamics (PFT dyn.), plant demography and the number of plant functional types. Natural plant functional types exclude agricultural crops and pasture.

estimated by IMAGE, only CESM2 utilized it of all the models in this study. Therefore, we consider *esm-ssp585-ssp126Lu* as having low forestation and would be representative of the lower end of the future mitigation potential from forestation.

2.2. Participating Models

Seven Earth system models participated in both LUMIP and C4MIP with simulations available for *esm-ssp585-ssp126Lu* and *esm-ssp585*. NorESM5 contributed a simulation to LUMIP for the *esm-ssp585-ssp126Lu* experiment, however, we have excluded it since it was run in concentration-driven mode. We also excluded BCC-CSM2-MR upon request of the developers due to a bug in the soil respiration. A brief overview of these models is presented in Table 1. Two models included wildfire schemes, three models included PFT dynamics (i.e., the geographical distribution of the vegetation types changes in response to environmental changes and competition modulated by physiological constraints), two models include plant demography (i.e., competition of vegetation age or height classes) and six models included nitrogen limitation. ACCESS-ESM1-5 is the only model to include phosphorus limitation. Furthermore, ACCESS-ESM1-5 is the only model to have multiple ensemble members available for both simulations, of which there are 10 for each experiment. The ACCESS-ESM1-5 ensemble members were generated by a branched initialization technique from the pre-industrial control simulation which runs throughout the historical period. The *esm-ssp585-ssp126Lu* and *esm-ssp585* simulations are initialized from the end of each of the historical ensemble members and the corresponding ensemble members are therefore necessarily paired together when the difference is taken.

CanESM5 has different ensemble initialization methods for *esm-ssp585* and *esm-ssp585-ssp126Lu*. The former uses r1i1p1f1 and the latter uses r1i1p2f1, which features recent bug-fixes in the model. To account for the slightly different initial conditions, the CanESM5 model (green line in Figure 3) has been bias corrected by subtracting the difference in the carbon pools between the reference and forestation simulations at the start of the experiment (2015). This makes the CanESM5 comparable with other models for all variables.

The forest and tree definition can still differ between models depending on how the LUH2 forcing data are translated into model PFTs. For example, CanESM5 and GFDL-ESM4 do not have an explicit representation of shrubs but consider them as tree PFTs and therefore areas otherwise considered as shrubs in other models would be included in treeFrac. Also, none of the models here have a representation of rangelands and thus the LUH2 rangelands can be variously interpreted by the models as forest, pasture, shrublands or savanna, which may or may not be considered as woody tree PFTs.

2.3. Data

The data used in this study are available from the Earth System Grid Federation. For each model, we use the following monthly mean variables: tree cover fraction (treeFrac), vegetation, litter, soil and total land carbon

(cVeg, cLitter, cSoil, cLand respectively), atmospheric CO_2 concentrations (co2), ocean CO_2 flux (fgco2), 1.5 m surface air temperature (tas) and precipitation rate (pr). From ACCESS-ESM1.5 we also use daily maximum temperatures (tasmax). Some variables are not available for particular models, such as treeFrac data from MIROC and atmospheric CO_2 concentration from GFDL-ESM4.

Changes in the treeFrac variable typically represent the changes in forests, but the definition of forest cover can vary. ESMs represent forest area as a fraction of a grid cell's land surface rather than crown cover, which is an important distinction since definitions of forests vary greatly with crown cover (Zomer et al., 2008).

2.4. Analysis and Statistical Methods

In this study, the analysis of results is done in two parts, a global mean analysis of CMIP6 models, and a regional analysis of the ACCESS-ESM1-5 10 member ensemble (since an ensemble allows for a more robust detection of noisy regional signals). For the global mean analysis across CMIP6 models, we analyze global forest cover fractions, terrestrial and oceanic carbon, surface air temperature and precipitation. We calculate trends in the difference of global mean temperatures and precipitation to examine the change in temperature as forests expand. For this, we use the Theil-Sen slope estimator and test its significance at the 5% level using the Mann-Kendall trend test.

For a more detailed analysis of regional carbon uptakes, the ACCESS-ESM1-5 regional analyses have been divided into 6 regions that feature notable changes in tree cover. These regions are shown in Figure 1c.

Much of the simulated tree cover changes between the two simulations occur in a handful of concentrated regions. Therefore, to examine the local scale impact of substantial forestation on temperature, histograms of the frequency distributions for specific grid points are calculated for the locations shown by the crosses in Figure 1. These large forestation regions are in Eastern North America (275°E, 37.5°N), East Asia (99.375°E, 32.5°N), and Amazonia (311.25°E, −12.5°N). The difference in the temperature distribution in the two simulations in response to forestation is tested using the 2-sample Kolmogorov-Smirnov test for the equality of distributions at the 5% level.

Lastly, to examine the relationship between forestation and climate, correlations were done on ensemble mean surface air temperature and tree fraction using the Spearman's rank correlation and the significance was tested at the 5% level (Kokoska & Zwillinger, 2000).

3. Results and Discussion

3.1. Global Multi-Model Inter-Comparison

3.1.1. Carbon Cycle

Each model has a unique representation of forests which results in a variety of changes in simulated global tree cover. This is demonstrated in Figure 2, which shows the difference in tree cover fraction between the two scenarios for each model at 2100 (Figure S2 in Supporting Information S1 also shows the temporal change for each experiment). The unique representations of forest cover arise from a variety of sources. Firstly, each model has various combinations of evergreen/deciduous broadleaf/needleleaf PFTs, sometimes in specific climates such as tropical, temperate and boreal regions. Modeling groups therefore must have diverse approaches to translating the natural lands from LUH2 into these model-specific PFTs differently. Secondly, each model has a different grid resolution, which causes large differences in forest areas when the cover fractions are remapped. Thirdly, each model may use a slightly different spatial distribution of potential vegetation, resulting in different forest areas when land-use changes are applied. Finally, UKESM1-0-LL, GFDL-ESM4 and MPI-ESM1-2-LR include PFT dynamics that respond to changes in climate, and these are the models that deviate from the LUH2 land-use forcing the most.

To interpret the difference in tree cover response of the models, it is helpful to be aware of some of the known climate and dynamic features of each model. Firstly, CanESM5 particularly stands out as having a net loss of tree area by 2100 (Figure 2a), however, this is due to CanESM5 lacking an explicit representation of shrubs and rangelands, which have been allocated as forest. Several show large-scale forest loss in some regions. The mechanisms that drive such forest loss in CMIP6 models are typically model-dependent climate sensitivities for prolonged drying under which models with PFT dynamics would favor the expansion of savanna or grass biomes, as well
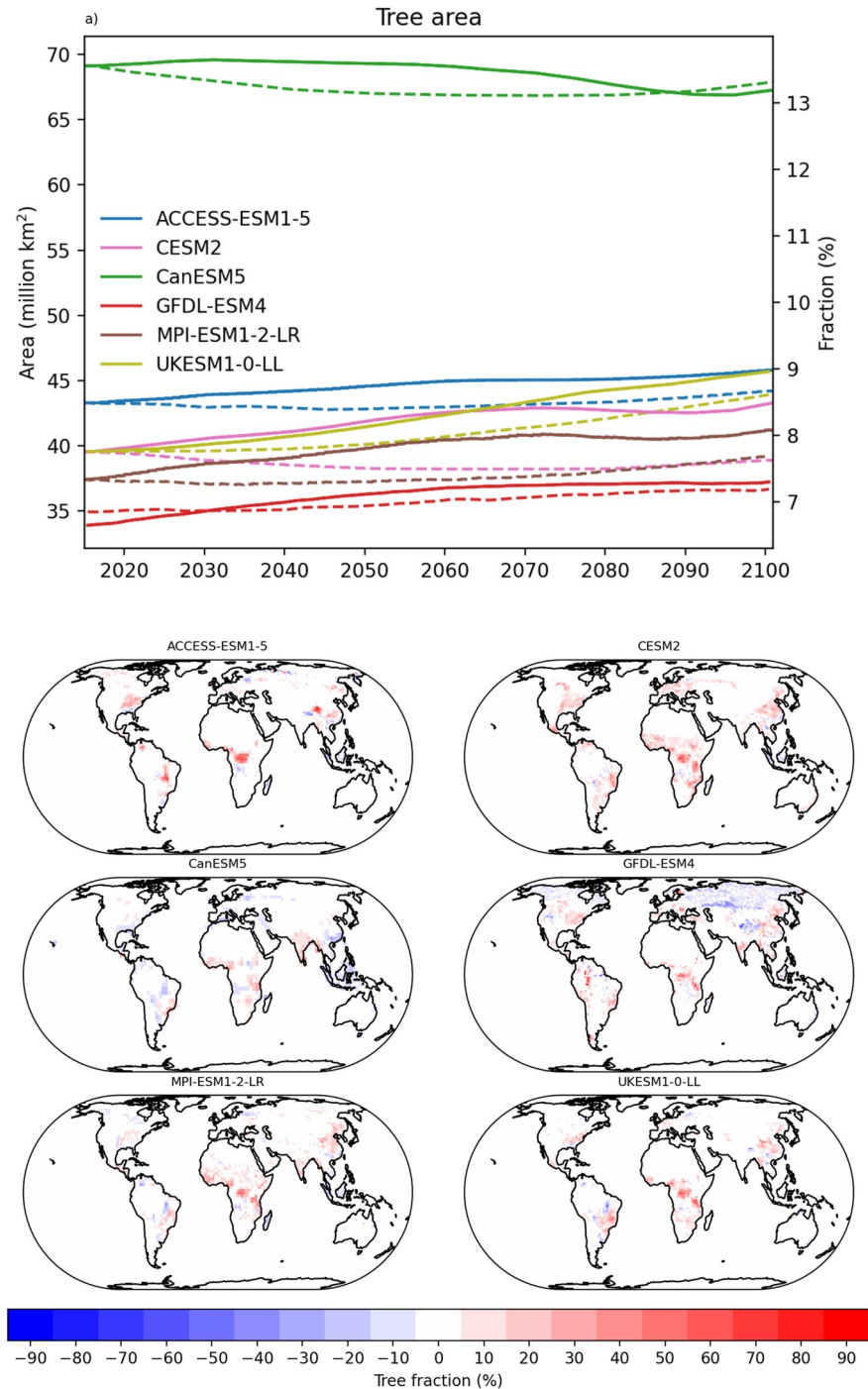
Figure 2. (a) Global sum tree cover area (or global mean area fraction for the right axis) over the period 2015 to 2100 in *esm-ssp585-ssp126Lu* (forestation) (solid) and *sss-ssp585* (reference) (dashed) for each model. (b)-(g) 2100 maps of tree cover fraction difference between the simulations for each model. MIROC-ES2L data for tree fraction are not available.

as disturbances from deforestation and fires (Cano et al., 2022; Parry et al., 2022). For example, CanESM5, MPI-ESM and UKESM1-0-LL also feature substantial Amazonian die-back in both scenarios (Figure S2 in Supporting Information S1), typically driven by localized drying. Secondly, MPI-ESM1-2-LR has large amounts of tree cover increase in semi-arid regions in Africa and Australia. Thirdly, the UKESM1-0-LL *esm-ssp585-ssp126Lu* scenario is known to have enhanced CO_2 fertilization compared to other models and warming in the mid-to high-latitudes resulting in increased tree cover fractions in Figure S2 in Supporting Information S1 and
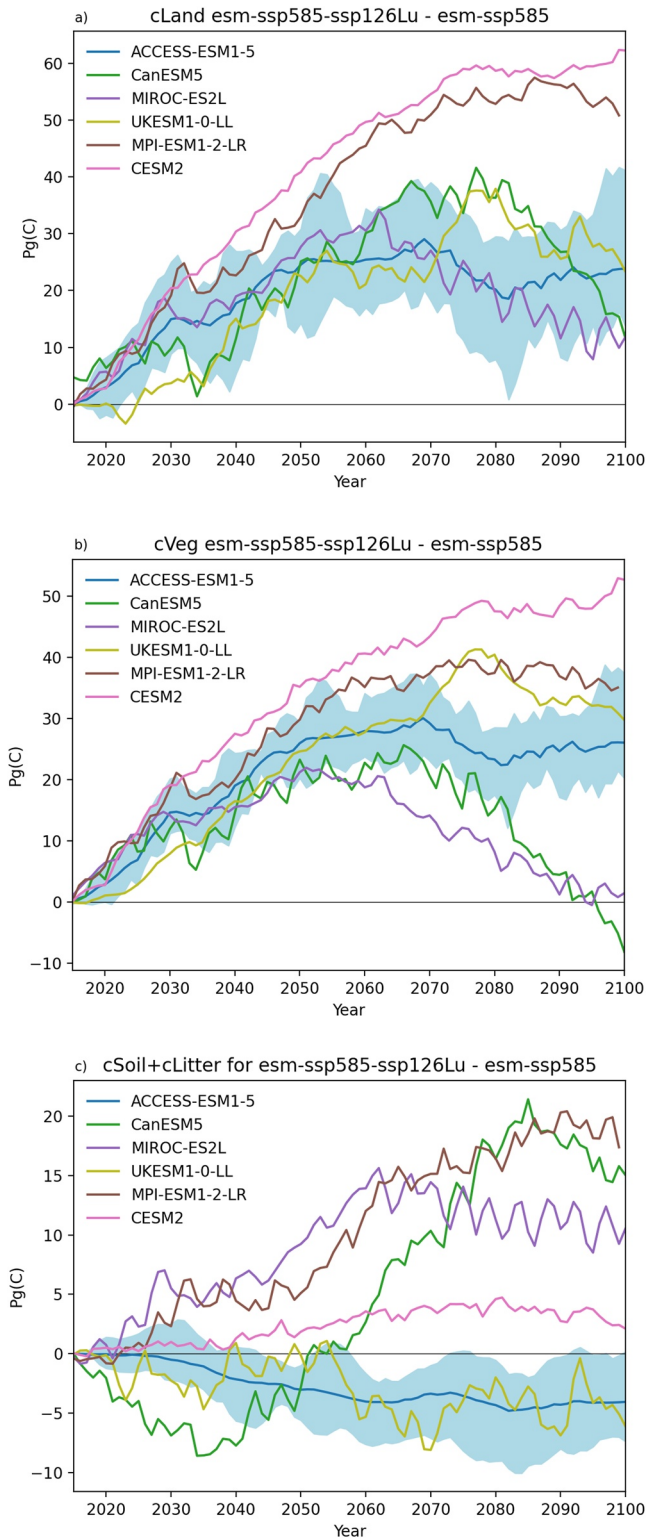
Figure 3. Differences for (a) total land carbon, (b) vegetation carbon and (c) litter and soil carbon (cLitter + cSoil) between *esm-ssp585-ssp126Lu* (forestation) and *esm-ssp585* (reference) for 6 CMIP6 models. ACCESS-ESM1-5 is plotted as the ensemble mean and the blue shading indicates the ensemble range. Data for GFDL-ESM4 carbon pools are not available.

decreased tree cover fraction in tropical South America and southeast Asia, driven by a combination of land use change and regional drying trends. Lastly, the tree cover changes in each model may not fully capture actual dynamics that may limit forest expansion. For example, models that do not include PFT dynamics may not represent natural encroachment of forests onto natural grasslands. Also, no models have mechanisms for seed dispersal to limit forest expansion, and seedling planting on managed lands is implicit rather than explicit. Depending on the ESM implementation, forests may take some time to grow their relevant pools. For example, ACCESS-ESM1-5 takes ~100 years for wood pools to stabilize following complete forestation on all croplands (not shown).

ACCESS-ESM1-5 is an example that closely follows the spatial distribution of the LUH2 land-use forcing. By 2100, ACCESS-ESM1-5 has a forest expansion of 1.59 million km² and agricultural abandonment of 1.11 million km². By mid-century, crops reach a minimum of 2.74 million km² less than in 2015, before rising again in the latter half of the century (Figures S3 and S4 in Supporting Information S1). Forestation is dominated by growth of evergreen broad leaf forests, followed by evergreen needle leaf forests, and deciduous broad leaf forests. Deciduous needle leaf forests only make up a small fraction of forests and do not show any expansion.

The inter-model spread in increased tree cover fraction corresponds to the spread of carbon uptake potentials into the terrestrial system. Figure 3 shows the change in the model's terrestrial carbon pools due to forestation. The increase in total land carbon tends to diminish toward the end of the century as new forest areas reach maturity. The models show a total CO_2 removal by the land surface between 10 and 60 Pg C by 2100. The ACCESS-ESM1-5 ensemble spread indicates that the internal climate variability can constitute a considerable portion of this range (between 10 and 40 Pg C). Such a large multi-model spread likely arises from the use of a very high emissions scenario, which amplifies the range of temperature responses since each model has a unique climate sensitivity. Models with strong climate-carbon feedbacks on land would further increase the spread of land carbon uptake.

For vegetation carbon, the models either maintain a carbon removal potential of ~20–50 Pg C by 2100 (ACCESS-ESM1-5, UKESM1-0-LL, MPI-ESM1-2-LR and CESM2), or the vegetation carbon gains by the middle of the century are lost to the atmosphere by 2100 (CanESM5 and MIROC-ES2L). ACCESS-ESM1-5 and UKESM1-0-LL lie approximately in the middle of the model spread. These models use different versions of the same atmosphere model and therefore share similar climate physics, however UKESM1-0-LL has a greater transient climate response (TCR) to forestation and atmospheric CO_2 changes.

Soil carbon shows varied responses to forestation, but most models show carbon accumulates in litter and soil pools and remain carbon sinks over the 21st century. For example, for CanESM5, even though there is a net loss of tree cover by 2100, much of the land carbon is stored in soil and litter. However, ACCESS-ESM1-5 and UKESM1-0-LL show decreases in soil carbon in response to forestation. For ACCESS-ESM1-5, this is likely due to differences in PFT-specific parameters for the proportion of litter carbon stored as lignin, as well as the litter and soil carbon turnover rates between forests, crops and grasses, with the former having slower turnover from litter to soil. This results in carbon accumulating in the litter pools and the soil carbon pools decay to a new lower equilibrium. In the UKESM1-0-LL,
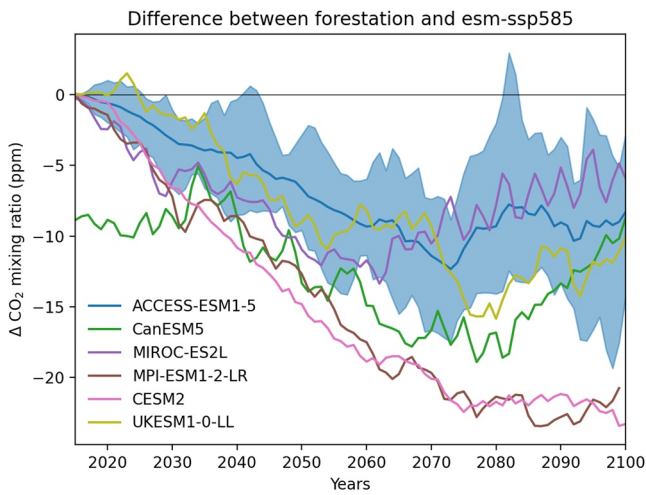
Figure 4. Difference in atmospheric CO_2 concentration between *esm-ssp585-ssp126Lu* (forestation) and *esm-ssp585* (reference). The ACCESS-ESM1-5 is plotted as the ensemble mean with the blue shading representing the ensemble range. CanESM5 does not start at 0 because of the different physics members highlighted in Section 2.2.

however, severe deforestation of tropical PFTs in the early part of SSP5-8.5 compared to SSP1-2.6 results in a large negative difference in litter and soil carbon mid-century. Much of the deforested wood is transferred to wood products, with less harvested carbon being transferred to soil in the esm-ssp585-ssp126Lu scenario.

An increased land surface sink results in a corresponding decrease in atmospheric CO_2 concentrations as demonstrated in Figure 4. The multi-model range is −5 to −22 ppm, with concentrations projected to increase from 400 to 1088 ppm under SSP5-8.5 (REMIND-MAGPIE in Figure S5 in Supporting Information S1). This change represents 0.7%–3% of the reduction required to return the CO_2 concentration at 2100 to that of the level in 2010. The largest change in concentration is ∼22 ppm from MPI-ESM1-2-LR, which is still much lower than the 85 ppm decrease in the scenario used by Sonntag et al. (2016). In that study, there was a much larger forestation of ∼9 million km² in the RCP4.5 scenario, compared to the ∼2 million km² for MPI-ESM here, which likely explains most of the difference. The ACCESS-ESM1-5 ensemble range demonstrates that atmospheric CO_2 is strongly sensitive to internal climate variability, encompassing 60% of the multi-model range.

3.1.2. Climate Response

Figure 5 shows that trends in global mean surface air temperature over the century are not significantly altered by forestation, which is likely because the forest area difference between the two scenarios is not large enough. Despite not being statistically significant, the global temperature trends disagree in sign, with most showing negative trends and ACCESS-ESM1-5, CanESM5 and CESM2 showing positive trends. The effect that internal climate variability can have on the trends is demonstrated by the ACCESS-ESM1-5 ensemble. While the ensemble mean trend showed no significant change, three members showed a significant positive trend. The CO_2 concentration of these three members is not consistently greater than the other ensemble members throughout the experiment (Figure S6 in Supporting
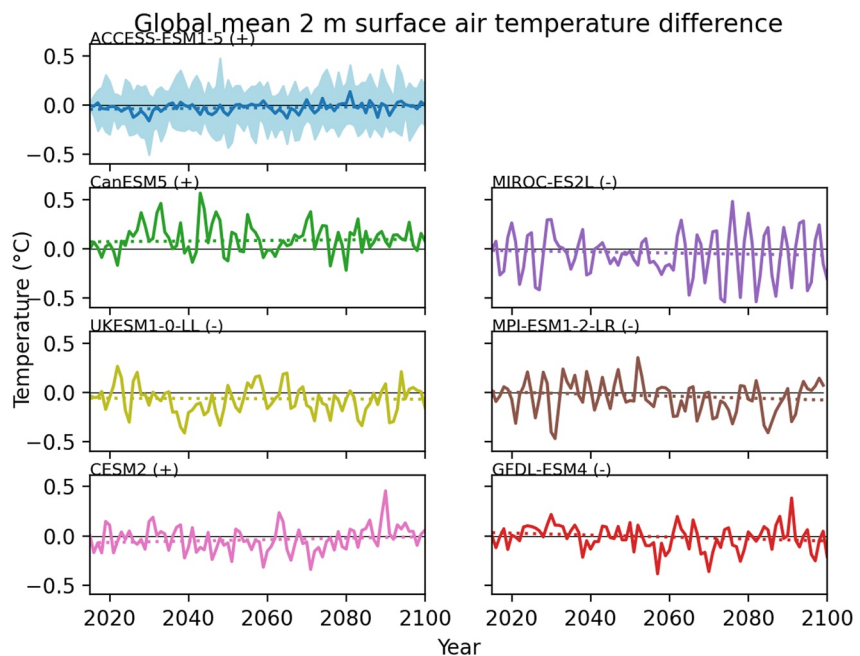

Figure 5. Difference in surface air temperature between *esm-ssp585-ssp126Lu* (forestation) and *esm-ssp585* (reference) (solid lines) and the corresponding trends (dotted). The blue shading is the ACCESS-ESM1-5 ensemble range. All trends are not statistically significant at the 5% level. The (+) and (−) symbols next to the model names denote the sign of the trend line.

Information S1), which indicates that the significance of the temperature decrease in these members is mostly driven by internal climate variability.

The temporal variance of temperature also shows unique behavior among the models. For example, MIROC-ES2L features large multi-annual oscillations in global mean temperature driven by large El Niño–Southern Oscillation amplitude that results in similar variability in global temperature (Hajima et al., 2020). This occurs in both the forestation scenario and the reference scenario (Figure S8 in Supporting Information S1), which causes large oscillations in the difference as they drift out of phase in the latter half of the century.

Similar to global mean surface air temperature, the response of global mean precipitation to forestation is also unclear from the models (Figure S9 in Supporting Information S1), with all models showing no significant trends in global precipitation rate.

3.2. Comparison of Temperature Impacts in Other Modeling Studies

Our results based on CMIP6 models agree well with (Sonntag et al., 2018) in sign but vary in the magnitude of the climate response. The Sonntag et al. (2018) study consists of only a single model that may have an incomplete representation of the real world. Therefore, a multi-model range provides a better view of these uncertainties. For example, MPI-ESM's high CO_2 uptake by vegetation may be due to missing natural disturbance processes such as insects, hydraulic failure and inclusion of PFT dynamics. Another example is CESM2, which does not have PFT dynamics, but it has high CO_2 uptake because it has a larger change in tree fraction than other models, since they included the additional tree cover provided by LUH2. An example of a low CO_2 uptake model is ACCESS-ESM1-5, which includes phosphorus limitation that potentially limits its CO_2 uptake and hence reduces its importance of global biogeochemical cooling.

The sensitivity of the model's global temperature change ranges from -0.16 (GFDL-ESM4) to $+0.019$ (ACCESS-ESM1-5) K per million km^2 of forestation. While GFDL-ESM4 had the largest sensitivity to forestation, it had the smallest temperature change and the smallest change in tree cover fraction. The sensitivity of CanESM5 and MPI-ESM1-2-LR agree well in sign and magnitude with the prior Sonntag et al. (2018) study, which used an earlier version of MPI-ESM. ACCESS-ESM1-5 and CESM2 contrast with the other models showing warming with forestation. This is more consistent with the sensitivities of deforestation from Boysen et al. (2020), if the global effects of forestation were simply the reverse of the effects of deforestation. However, the *deforest-glob* experiment used in Boysen et al. (2020) are simulations with constant pre-industrial CO_2 concentrations and therefore does not include biogeochemical feedbacks.

To estimate what the impact on global temperatures from only CO_2 would be, Table 2 also shows the transient climate response of the models taken from Arora et al. (2020), and in the following columns is the calculation of the expected change in temperature from only the change in atmospheric concentration shown in Figure 4. In the last column is the net change in global temperature from both biogeochemical and biogeophysical processes as taken from the trends in Figure 5. Most models have a smaller decrease in global temperatures in response to CO_2 decreases associated with forestation than what would be expected from their TCR alone, suggesting that the biogeophysical effects of forestation increase global temperatures and offset the potential biogeochemical cooling.

3.3. Regional Land Carbon and Climate Responses in ACCESS-ESM1.5

3.3.1. Overview of ACCESS-ESM1.5 Response to Forestation

Since ACCESS-ESM1-5 has 10 ensemble members available, and the regional distribution of new forest growth varies greatly among the models, the regional analysis will focus only on ACCESS-ESM1-5. The single model ensemble allows us to examine the impact of forestation on the probability distribution of regional surface temperatures and carbon uptake. The carbon cycle in ACCESS-ESM1-5 in the forestation scenario reflects the forestation in the forcing data well (Figure 6a), with the land surface acting as a sink in the first half of the century when most of the forestation occurs and becoming a weak source toward the end of the century. The ocean sink strengthens as the partial pressure of CO_2 on the ocean surface increases throughout the century from increasing atmospheric CO_2 concentrations. However, the lower atmospheric CO_2 concentrations relative to the reference simulation results in the ocean absorbing cumulatively $\sim1.3 \pm 0.5$ Pg C less by 2100 (Figure 6b). Globally,

Table 2
Comparison of CMIP6 Forestation to Other Modeling Studies

	Model	Area	ΔT	ΔT/Mkm²	TCR	PI CO₂	For. ΔCO₂	Exp. ΔT from TCR
CMIP6 Forestation	ACCESS-ESM1-5	1.6	0.031	0.019	2.15	284	−9	−0.068
	CESM2	4.4	0.062	0.014	2.29	280	−21	−0.171
	CanESM5	−0.6	0.026	−0.042	2.54			
	MPI-ESM1-2-LR	2	−0.084	−0.041	1.86	278	−22	−0.147
	MIROC-ES2L		−0.049		1.58	280.3	−6	−0.034
	UKESM1-0-LL	2	−0.011	−0.005	2.42	284	−10	−0.085
	GFDL-ESM4	0.52	−0.083	−0.161				
Sonntag et al. (2018)	MPI-ESM-LR	9	−0.27	−0.03				
Boysen et al. (2020)	MPI-ESM1-2-LR	−20	−0.04	0.002				
	CESM2	−20	−0.02	0.001				
	CanESM5	−20	−0.55	0.0275				
	MIROC-ES2L	−20	−0.01	0.0005				
	UKESM1-0-LL	−20	−0.51	0.0255				

Note. Change in temperature from forestation normalized by the area of deforestation (Boysen et al., 2020), compared to values taken from (Sonntag et al., 2018) forestation study and the CMIP6 forestation presented in Figure 5. Model transient climate response and expected change in temperature. TCR is the transient climate response of each model taken from Aurora et al. (2020), PI CO₂ is the model's simulated preindustrial concentration, For. CO₂ is the change in atmospheric CO₂ concentration from Figure 4.

cLand increases by $1.3 \pm 0.3\%$ of the cLand in the reference simulation, with $3.3 \pm 0.4\%$ increase in cVeg and $0.5 \pm 3\%$ decrease in cSoil. ACCESS-ESM1-5 is also the only model to include phosphorus nutrient limitation, and therefore the ACCESS-ESM1-5 cVeg pools contrasts to other models, reaching a stable limit by 2100 (Figure S10a in Supporting Information S1) while other model's cVeg are still increasing by 2100. The climate in both the forestation and reference simulations are similar, with a warming of ~4°C by 2100 and precipitation increases by 0.216 kg m⁻² day⁻¹.

3.3.2. Regional Changes in Vegetation and Climate Extremes

The scenario difference in treeFrac for each region in shown in Figure 7a and demonstrates the extent of forestation that occurs in these regions. The Central Africa region has the largest difference in forest cover extent. The Eastern North America region has an initial rapid increase in forest cover, followed by a dip of forest loss later in the century before recovering again. The Amazon, East Asia, and Boreal North America regions have a steady increase in forest cover throughout the century. Finally, the Boreal Eurasia undergoes a small amount of forest increase followed by forest loss.
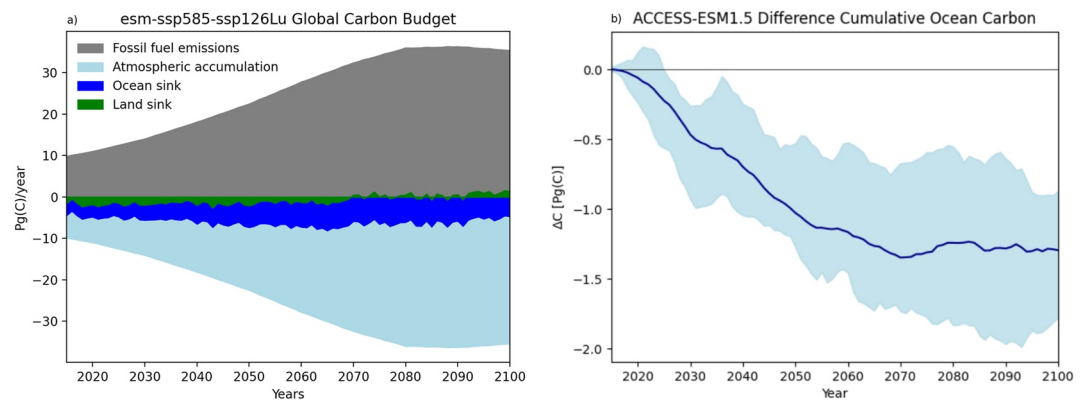

Figure 6. (a) Carbon budget of global fluxes of fossil fuel emissions and the natural sinks for the land (net-land-atmosphere exchange as the sum of the natural terrestrial sink and land-use change fluxes), ocean and atmospheric accumulation. (b) The cumulative ocean carbon difference between *esm-ssp585-ssp126Lu* (forestation) and *esm-ssp585* (reference).
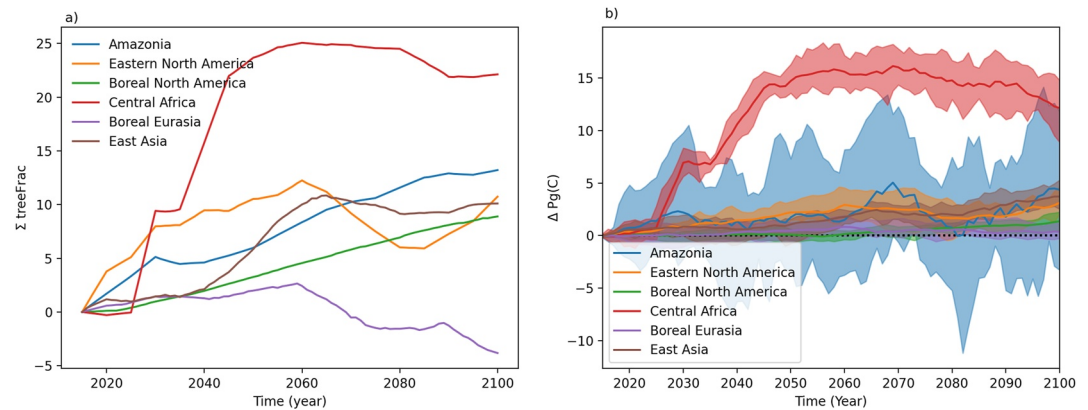
Figure 7. Differences between *esm-ssp585-ssp126Lu* (forestation) and *esm-ssp585* (reference) for (a) sum of the treeFrac in each region in Figure 1 and (b) total land carbon content for each region in Figure 1, based on results from ACCESS-ESM1-5.

These forest cover changes largely determine the uptake of carbon by the land, but with considerable variability within each region. Figure 7b shows the change in total land carbon for each of the regions outlined in Figure 1c. There are increases in land carbon for all regions and ensemble members except Amazonia, where some ensemble members show a small decrease in cVeg by 2100, due to internal climate variations. The region with the largest change in land carbon content is Central Africa (Figure 7), however this difference is due to avoided deforestation that occurs in the reference simulation, rather than due to new forest growth in the forestation experiment (Figure S3a and S3b in Supporting Information S1). This highlights the importance of including avoided deforestation in future long-term national climate strategies, not just to avoid related CO_2 emissions from the burning and decay of biomass and soil carbon, but also since a considerable portion of land-use emissions comes from the loss of additional sink capacity from deforestation (Gitz & Ciais, 2003; Obermeier et al., 2021; Pongratz et al., 2014). The increased land sink from the combined effect of forestation and CO_2 fertilization are partially offset by the increase in soil respiration (Figure S10b in Supporting Information S1), particularly in Australia where there is no increase in forest cover in the SSP1-2.6 scenario.

The relationship of surface air temperature and changes in total tree cover fraction varies substantially by region. For example, in Figure 8, the correlation of temperature and tree cover fraction is positive in the tropical regions of Central Africa, South America, the Maritime Continent, and East Asia. Hence, increased tree cover fraction increases surface air temperature and the effect of decreased surface albedo dominates. In contrast, some areas immediately surrounding the avoided deforestation region of Central Africa show the opposite effect, whereby increased tree cover negatively correlates with air temperature and hence the cooling effect of evapotranspiration dominates. Furthermore, in the sub-tropical and boreal regions of eastern North America, the correlation is negative, indicating that as forest cover increases, temperature decreases.

The net effect of growing trees in the tropical regions is that it causes localized warming at the extreme ends of the temperature distributions. For specific grid points with large changes from grass to tree biomes, the distribution of summer daily maximum surface air temperature for both the forestation and reference simulations are shown in Figure 9. The Amazon grid-point features changes in mostly C4 grass to evergreen broad leaf forest, representing an increase in tree cover fraction of 60%. This corresponds to a statistically significant change in the distribution, particularly for temperatures greater than 50°C (Figure 9b).

The increase in the high end of the temperature distributions in response to forestation are not consistent for all regions. For example, the large increase in forest cover for the grid point in Asia corresponds to a decrease in days greater than 23°C, while temperatures 17–23°C increase (Figure 9d), as the distribution gets narrower with forestation. The changes in daily maximum temperature at the lower end of the distribution in response to forestation are much more regionally consistent, showing a decrease in cooler than average days for both the Amazon grid point and the Asia Grid point.

Some regions show decreases in surface air temperature in response to increasing tree cover. Of particular note is North America which features a large transition from C3 crops to deciduous broadleaf (Figure 9e). In ACCESS-ESM1-5, deciduous broad leaf forests have the highest reflectance of all the PFTs. The resulting
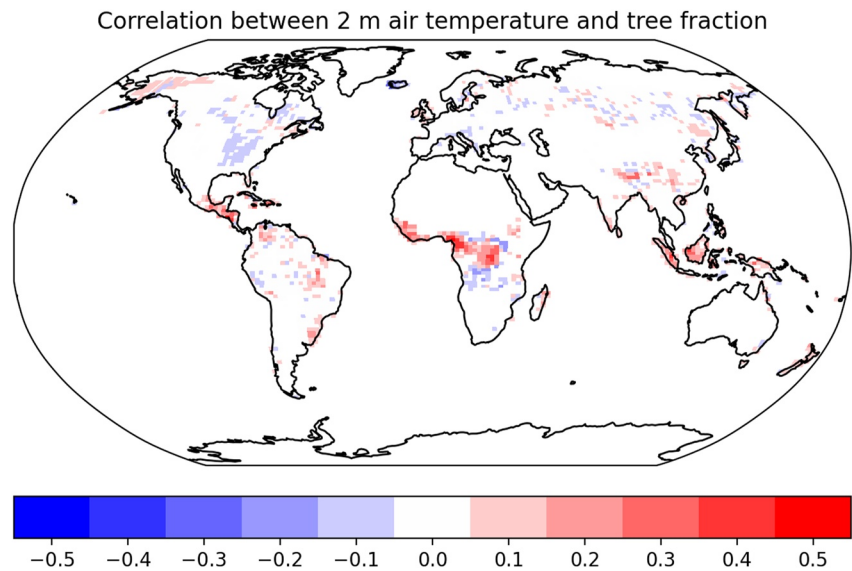
Correlation between 2 m air temperature and tree fraction

Figure 8. Correlation of ensemble mean 2 m surface air temperature difference with tree cover fraction difference (both *esm-ssp585-ssp126Lu-esm-ssp585*) in ACCESS-ESM1-5. Only statistically significant correlations at the 5% level are shown.

distribution shows decreases in the number of warm days and increased cool days in the forestation experiment (Figure 9f).

These results include both biogeochemical and biogeophysical effects of forestation on climate. Unfortunately, a biogeochemical-biogeophysical separation of the climate impacts of forestation cannot be made with the simulations available in LUMIP and C4MIP alone. To address this, future studies on forestation scenarios should include a corresponding concentration-driven simulation that uses the CO_2 concentrations from a forestation simulations with fully interactive carbon cycle, so that at least a biogeochemical-biogeophysical separation can be made.

4. Concluding Remarks

We conducted a multi-model intercomparison of a scenario for forestation as a means of CO_2 removal. This forestation scenario features high fossil fuel emissions, a much warmer climate and forestation and agricultural abandonment. The models show a diverse interpretation of the spatial patterns of forestation, and as a result, show a large range of outcomes for long-term carbon storage in forests. Four models show a stable but limited carbon sink by 2100, while two models show that the mitigation gains from forestation in the middle of the century will be mostly lost by 2100 under such a high warming scenario.

The change in atmospheric CO_2 concentrations from forestation only accounts for 0.7%–3% of the reduction required to return the SSP5-8.5 concentrations at 2100 to those at 2010. Hence, the models indicate that this amount of forestation results in only a small impact on global climate when combined with high fossil fuel emissions. The forestation also causes a shift in the global carbon balance, whereby increased uptake of carbon on the land of ~25 Pg C by 2100 results in a decrease in the uptake of carbon by the ocean in the ACCESS-ESM1-5 ensemble. Furthermore, ACCESS-ESM1-5 simulations show some increases in local-scale temperatures in locations where forestation occurs, while other regions show cooling. However, a key limitation of the experimental design of this study is that we cannot further decompose the ensemble spread of all the models into biogeochemical, and local/non-local biogeophysical components without additional simulations, such as those in Winckler, Lejeune, et al. (2019).

The scenario used in this study is specific to a world of extreme CO_2 emissions and does not consider the case where a significant reduction in fossil fuel emissions occurs. It is therefore still unclear how much more or less carbon would be sequestered by the terrestrial ecosystem under a cooler climate that would occur in conjunction with the expected emissions reduction efforts in the future. Therefore, future studies should aim to explore the
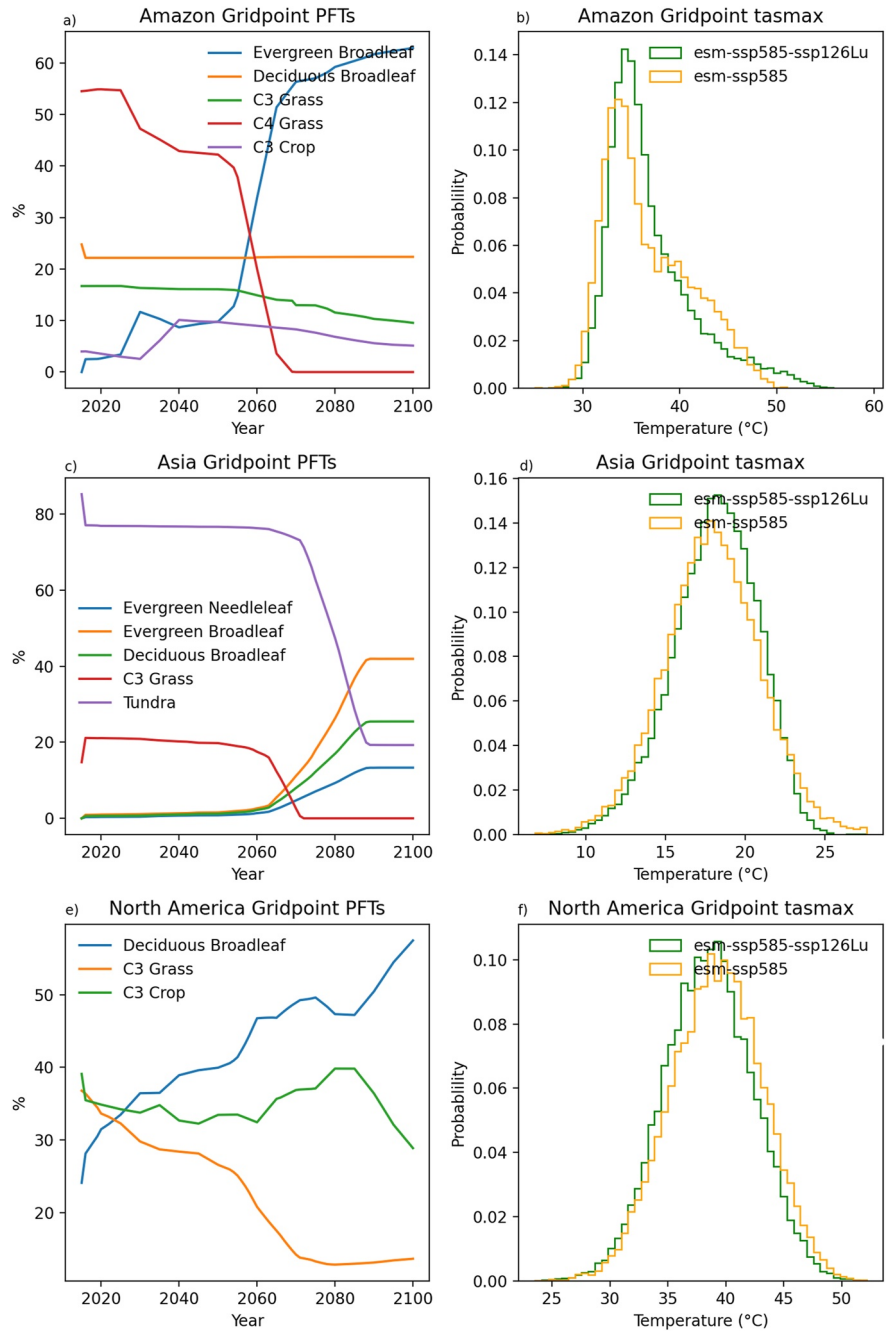
Figure 9. Cover fractions of plant functional types for ACCESS-ESM1-5 in *esm-ssp585-ssp126Lu* (a, c, e) for one selected grid point at the three locations marked in Figure 1c (Eastern North America (275°E, 37.5°N), East Asia (99.375°E, 32.5°N), and Amazonia (311.25°E, −12.5°N)). Distributions of summer time (June–August or December–February) maximum daily temperature for the last 20 years (b, d, f) of *esm-ssp585-ssp126Lu* (forestation) (green) and *esm-ssp585* (reference) (yellow).

effects of forestation for climate states under different target warming levels that are consistent with the Paris Agreement (e.g., King et al., 2021).

While the model projections in this study show that the modest amount of forestation under a very high emissions scenario has limited climate mitigation potential, this does not mean that forestation should not play a role in climate mitigation. Despite the limits, we also stress the importance of forestation on the local climate, since the impact of cooling or warming from forest expansion can affect extreme temperatures which can vary greatly by region. In addition to climate benefits, forestation and forest management provide a broad range of co-benefits

such as increased habitat, biodiversity and soil protection, and many of these features are not yet simulated in Earth system models, nor is the additional benefit of these ecosystem services accounted for in climate policies. For forestation to be an efficient long-term CO_2 removal strategy, it must also exist in conjunction with other strategies. By first regrowing forests for the purpose of CO_2 removal, forestation increases the natural land-based carbon and enables further development and supply of feedstock for human activity, including for climate mitigation (Geng et al., 2017). Forests that are sustainably harvested and regrown to remove CO_2 act as low-risk and cost-effective long-term carbon sinks, both in soils and in harvested wood products (Schulze et al., 2020; Soimakallio et al., 2021). Vegetation carbon may be lost in individual natural disturbance events such as fires, but the historically removed carbon remains locked. None of the models in this study (and very few in general) fully implement nature- and technology-based removal strategies, and therefore do not account for forest plantations, for example, to be further leveraged as in bio-energy sources along with carbon capture and storage. Since forestation (in particular forest management) and bio-energy usage are key assumptions of many low-emissions SSP scenarios to replace fossil fuels, implementing them in the Earth system modeling context is important for future research, along with more emphasis on the evaluation of different land-based mitigation pathways in low emission scenarios.

Abbreviation

C4MIP	Coupled Climate-Carbon Cycle Model Intercomparrison Project
CMIP6	Climate Model Intercomparrison six
DECK	Diagnostic, Evaluation and Characterization of Klima
LUH2	Land-Use Harmonization version two
LUMIP	Land-Use Model Intercomparrison Project
PFT	Plant functional type
RCP	Representative Concentration Pathway
SSP	Shared socio-economic pathway
SSP5-8.5	High fossil fuel emissions scenario
SSP1-2.6	Low fossil fuel emissions scenario with forestation
TCR	Transient climate response

Data Availability Statement

CMIP6 data used in this study are available from the Earth System Grid Federation (ESGF) (Cinquini et al., 2014). ACCESS-ESM daily data are stored on the National Computational Infrastructure Australia and are also available from the ESGF. Analysis scripts and post processed data for reproducing figures are available at https://doi.org/10.5281/zenodo.8429275 (Loughran, 2023).

References

Alkama, R., & Cescatti, A. (2016). Biophysical climate impacts of recent changes in global forest cover. *Science*, *351*(6273), 600–604. https://doi.org/10.1126/science.aac8083

Argles, A. P. K., Moore, J. R., & Cox, P. M. (2022). Dynamic Global Vegetation Models: Searching for the balance between demographic process representation and computational tractability. *PLOS Climate*, *1*(9), e0000068. https://doi.org/10.1371/journal.pclm.0000068

Arora, V. K., & Boer, G. J. (2005). A parameterization of leaf phenology for the terrestrial ecosystem component of climate models. *Global Change Biology*, *11*(1), 39–59. https://doi.org/10.1111/j.1365-2486.2004.00890.x

Arora, V. K., Katavouta, A., Williams, R. G., Jones, C. D., Brovkin, V., Friedlingstein, P., et al. (2020). Carbon–concentration and carbon–climate feedbacks in CMIP6 models and their comparison to CMIP5 models. *Biogeosciences*, *17*(16), 4173–4222. https://doi.org/10.5194/bg-17-4173-2020

Babiker, M., Berndes, G., Blok, K., Cohen, B., Cowie, A., Geden, O., et al. (2022). Cross-sectoral perspectives. In IPCC, 2022: Climate change 2022: Mitigation of climate change. Contribution of Working group III to the Sixth assessment Report of the Intergovernmental Panel on climate change. https://doi.org/10.1017/9781009157926.005

Bala, G., Caldeira, K., Wickett, M., Phillips, T. J., Lobell, D. B., Delire, C., & Mirin, A. (2007). Combined climate and carbon-cycle effects of large-scale deforestation. *Proceedings of the National Academy of Sciences*, *104*(16), 6550–6555. https://doi.org/10.1073/pnas.0608998104

Best, M. J., Pryor, M., Clark, D. B., Rooney, G. G., Essery, R. L. H., Ménard, C. B., et al. (2011). The Joint UK land environment simulator (JULES), model description – Part 1: Energy and water fluxes. *Geoscientific Model Development*, *4*(3), 677–699. https://doi.org/10.5194/gmd-4-677-2011

Betts, R. A. (2000). Offset of the potential carbon sink from boreal forestation by decreases in surface albedo. *Nature*, *408*(6809), 187–190. https://doi.org/10.1038/35041545

Betts, R. A. (2001). Biophysical impacts of land use on present-day climate: Near-surface temperature change and radiative forcing. *Atmospheric Science Letters*, *2*(1–4), 39–51. https://doi.org/10.1006/asle.2001.0037

Boysen, L. R., Brovkin, V., Pongratz, J., Lawrence, D. M., Lawrence, P., Vuichard, N., et al. (2020). Global climate response to idealized deforestation in CMIP6 models. *Biogeosciences*, *17*(22), 5615–5638. https://doi.org/10.5194/bg-17-5615-2020

Bright, R. M., Davin, E., O'Halloran, T., Pongratz, J., Zhao, K., & Cescatti, A. (2017). Local temperature response to land cover and management change driven by non-radiative processes. *Nature Climate Change*, *7*(4), 296–302. https://doi.org/10.1038/nclimate3250

Burton, C., Betts, R., Cardoso, M., Feldpausch, T. R., Harper, A., Jones, C. D., et al. (2019). Representation of fire, land-use change and vegetation dynamics in the Joint UK Land Environment Simulator vn4.9 (JULES). *Geoscientific Model Development*, *12*(1), 179–193. https://doi.org/10.5194/gmd-12-179-2019

Cano, I. M., Shevliakova, E., Malyshev, S., John, J. G., Yu, Y., Smith, B., & Pacala, S. W. (2022). Abrupt loss and uncertain recovery from fires of Amazon forests under low climate mitigation scenarios. *Proceedings of the National Academy of Sciences*, *119*(52), e2203200119. https://doi.org/10.1073/pnas.2203200119

Cinquini, L., Crichton, D., Mattmann, C., Harney, J., Shipman, G., Wang, F., et al. (2014). The Earth System Grid Federation: An open infrastructure for access to distributed geospatial data [dataset]. Future Generation Computer Systems, *36*, 400–417. https://doi.org/10.1016/j.future.2013.07.002

Danabasoglu, G., Lamarque, J., Bacmeister, J., Bailey, D. A., DuVivier, A. K., Edwards, J., et al. (2020). The Community earth system model version 2 (CESM2). *Journal of Advances in Modeling Earth Systems*, *12*(2). https://doi.org/10.1029/2019ms001916

Davin, E. L., & De Noblet-Ducoudré, N. (2010). Climatic impact of global-scale deforestation: Radiative versus Nonradiative processes. *Journal of Climate*, *23*(1), 97–112. https://doi.org/10.1175/2009jcli3102.1

De Hertog, S. J., Havermann, F., Vanderkelen, I., Guo, S., Luo, F., Manola, I., et al. (2022). The biogeophysical effects of idealized land cover and land management changes in Earth System Models. *Earth System Dynamics*. https://doi.org/10.5194/esd-13-1305-2022

Di Vittorio, A. V., Chini, L. P., Bond-Lamberty, B., Mao, J., Shi, X., Truesdale, J., et al. (2014). From land use to land cover: Restoring the afforestation signal in a coupled integrated assessment–earth system model and the implications for CMIP5 RCP simulations. *Biogeosciences*, *11*(22), 6435–6450. https://doi.org/10.5194/bg-11-6435-2014

Dunne, J. P., Horowitz, L. W., Adcroft, A. J., Ginoux, P., Held, I. M., John, J. G., et al. (2020). The GFDL earth system model version 4.1 (GFDL-ESM 4.1): Overall coupled model description and simulation Characteristics. *Journal of Advances in Modeling Earth Systems*, *12*(11). https://doi.org/10.1029/2019ms002015

Eyring, V., Bony, S., Meehl, G. A., Senior, C. A., Stevens, B., Stouffer, R. J., & Taylor, K. E. (2016). Overview of the coupled model intercomparison Project phase 6 (CMIP6) experimental design and organization. *Geoscientific Model Development*, *9*(5), 1937–1958. https://doi.org/10.5194/gmd-9-1937-2016

FAO. (2020). *Global forest resources assessment 2020*. Author. Retrieved from http://www.fao.org/documents/card/en/c/ca9825en

Fisher, R. A., Koven, C. D., Anderegg, W. R. L., Christoffersen, B. O., Dietze, M. C., Farrior, C. E., et al. (2018). Vegetation demographics in earth system models: A review of progress and priorities. *Global Change Biology*, *24*(1), 35–54. https://doi.org/10.1111/gcb.13910

Friedlingstein, P., Jones, M. W., O'Sullivan, M., Andrew, R. M., Bakker, D. C. E., Hauck, J., et al. (2022). Global carbon budget 2021. *Earth System Science Data*, *14*(4), 1917–2005. https://doi.org/10.5194/essd-14-1917-2022

Geng, A., Yang, H., Chen, J., & Hong, Y. (2017). Review of carbon storage function of harvested wood products and the potential of wood substitution in greenhouse gas mitigation. *Forest Policy and Economics*, *85*, 192–200. https://doi.org/10.1016/j.forpol.2017.08.007

Gitz, V., & Ciais, P. (2003). Amplifying effects of land-use change on future atmospheric CO_2 levels: Amplifying land-use effects ON atmospheric CO_2 levels. *Global Biogeochemical Cycles*, *17*(1). https://doi.org/10.1029/2002gb001963

Griscom, B. W., Adams, J., Ellis, P. W., Houghton, R. A., Lomax, G., Miteva, D. A., et al. (2017). Natural climate solutions. *Proceedings of the National Academy of Sciences*, *114*(44), 11645–11650. https://doi.org/10.1073/pnas.1710465114

Hajima, T., Watanabe, M., Yamamoto, A., Tatebe, H., Noguchi, M. A., Abe, M., et al. (2020). Development of the MIROC-ES2L Earth system model and the evaluation of biogeochemical processes and feedbacks. *Geoscientific Model Development*, *13*(5), 2197–2244. https://doi.org/10.5194/gmd-13-2197-2020

Harman, I., Bodman, R., Dix, M., & Srbinovsky, J. (2019). *CABLE within ACCESS-CM2 (Tech. Rep.)*. CSIRO. Retrieved from https://trac.nci.org.au/trac/cable/raw-attachment/wiki/CableDocuments/Harman_2019_CoE_final_report_revised.pdf

Hong, T., Wu, J., Kang, X., Yuan, M., & Duan, L. (2022). Impacts of different land Use scenarios on future global and regional climate extremes. *Atmosphere*, *13*(6), 995. https://doi.org/10.3390/atmos13060995

House, J. I., Colin Prentice, I., & Le Quéré, C. (2002). Maximum impacts of future reforestation or deforestation on atmospheric CO_2: MAXIMUM REFORESTATION and DEFORESTATION. *Global Change Biology*, *8*(11), 1047–1052. https://doi.org/10.1046/j.1365-2486.2002.00536.x

Hurtt, G. C., Chini, L., Sahajpal, R., Frolking, S., Bodirsky, B. L., Calvin, K., et al. (2020). Harmonization of global land use change and management for the period 850–2100 (LUH2) for CMIP6. *Geoscientific Model Development*, *13*(11), 5425–5464. https://doi.org/10.5194/gmd-13-5425-2020

Ito, A., & Hajima, T. (2020). Biogeophysical and biogeochemical impacts of land-use change simulated by MIROC-ES2L. *Progress in Earth and Planetary Science*, *7*(1), 54. https://doi.org/10.1186/s40645-020-00372-w

Ito, A., Hajima, T., Lawrence, D. M., Brovkin, V., Delire, C., Guenet, B., et al. (2020). Soil carbon sequestration simulated in CMIP6-LUMIP models: Implications for climatic mitigation. *Environmental Research Letters*, *15*(12), 124061. https://doi.org/10.1088/1748-9326/abc912

Ito, A., & Inatomi, M. (2012). Water-use efficiency of the terrestrial biosphere: A model analysis focusing on interactions between the global carbon and water cycles. *Journal of Hydrometeorology*, *13*(2), 681–694. https://doi.org/10.1175/jhm-d-10-05034.1

Jones, C. D., Arora, V., Friedlingstein, P., Bopp, L., Brovkin, V., Dunne, J., et al. (2016). C4MIP – The coupled climate–carbon cycle model intercomparison Project:experimental protocol for CMIP6. *Geoscientific Model Development*, *9*(8), 2853–2880. https://doi.org/10.5194/gmd-9-2853-2016

King, A. D., Sniderman, J. M. K., Dittus, A. j., Brown, J. R., Hawkins, E., & Ziehn, T. (2021). Studying climate stabilization at Paris Agreement levels. *Nature Climate Change*, *11*(12), 1006–1013. https://doi.org/10.1038/s41558-021-01225-0

Klein Goldewijk, K. (2001). Estimating global land use change over the past 300 years: The HYDE Database. *Global Biogeochemical Cycles*, *15*(2), 417–433. https://doi.org/10.1029/1999gb001232

Kokoska, S., & Zwillinger, D. (2000). *Crc standard probability and statistics tables and formulae* (student edition). Taylor & Francis. Retrieved from https://books.google.com.au/books?id=G5hJqwjweiUC

Kowalczyk, E. A., Wang, Y. P., Law, R. M., Davies, H. L., McGregor, J. L., & Abramowitz, G. (2006). The CSIRO Atmosphere Biosphere Land Exchange (CABLE) model for use in climate models and as an offline model (p. 42).

Kumar, S., Dirmeyer, P. A., Merwade, V., DelSole, T., Adams, J. M., & Niyogi, D. (2013). Land use/cover change impacts in CMIP5 climate simulations: A new methodology and 21st century challenges: LU change impacts in CMIP5. *Journal of Geophysical Research: Atmospheres*, *118*(12), 6337–6353. https://doi.org/10.1002/jgrd.50463

Lawrence, D. M., Fisher, R. A., Koven, C. D., Oleson, K. W., Swenson, S. C., Bonan, G., et al. (2019). The Community land model version 5: Description of new features, Benchmarking, and impact of forcing uncertainty. *Journal of Advances in Modeling Earth Systems*, *11*(12), 4245–4287. https://doi.org/10.1029/2018ms001583

Lawrence, D. M., Hurtt, G. C., Arneth, A., Brovkin, V., Calvin, K. V., Jones, A. D., et al. (2016). The land Use model intercomparison Project (LUMIP) contribution to CMIP6:rationale and experimental design. *Geoscientific Model Development*, *9*(9), 2973–2998. https://doi.org/10.5194/gmd-9-2973-2016

Lee, X., Goulden, M. L., Hollinger, D. Y., Barr, A., Black, T. A., Bohrer, G., et al. (2011). Observed increase in local cooling effect of deforestation at higher latitudes. *Nature*, *479*(7373), 384–387. https://doi.org/10.1038/nature10588

Lenton, T. M., & Vaughan, N. E. (2009). The radiative forcing potential of different climate geoengineering options. *Atmospheric Chemistry and Physics*, *23*(15), 5539–5561. https://doi.org/10.5194/acp-9-5539-2009

Li, Y., Zhao, M., Mildrexler, D. J., Motesharrei, S., Mu, Q., Kalnay, E., et al. (2016). Potential and Actual impacts of deforestation and afforestation on land surface temperature. *Journal of Geophysical Research: Atmospheres*, *121*(24). https://doi.org/10.1002/2016jd024969

Loughran, T. F. (2023). tammasloughran/afforestation [software]. Zenodo. https://doi.org/10.5281/zenodo.8429275

Luyssaert, S., Jammet, M., Stoy, P. C., Estel, S., Pongratz, J., Ceschia, E., et al. (2014). Land management and land-cover change have impacts of similar magnitude on surface temperature. *Nature Climate Change*, *4*(5), 389–393. https://doi.org/10.1038/nclimate2196

Mauritsen, T., Bader, J., Becker, T., Behrens, J., Bittner, M., Brokopf, R., et al. (2019). Developments in the MPI-M earth system model version 1.2 (MPI-ESM1.2) and its response to increasing CO_2. *Journal of Advances in Modeling Earth Systems*, *11*(4), 998–1038. https://doi.org/10.1029/2018ms001400

Obermeier, W. A., Nabel, J. E. M. S., Loughran, T., Hartung, K., Bastos, A., Havermann, F., et al. (2021). Modelled land use and land cover change emissions – A spatio-temporal comparison of different approaches. *Earth System Dynamics*, *12*(2), 635–670. https://doi.org/10.5194/esd-12-635-2021

O'Neill, B. C., Tebaldi, C., Van Vuuren, D. P., Eyring, V., Friedlingstein, P., Hurtt, G., et al. (2016). The scenario model intercomparison Project (ScenarioMIP) for CMIP6. *Geoscientific Model Development*, *9*(9), 3461–3482. https://doi.org/10.5194/gmd-9-3461-2016

Parry, I. M., Ritchie, P. D. L., & Cox, P. M. (2022). Evidence of localised Amazon rainforest dieback in CMIP6 models. *Earth System Dynamics*, *13*(4), 1667–1675. https://doi.org/10.5194/esd-13-1667-2022

Pongratz, J., Reick, C. H., Houghton, R. A., & House, J. I. (2014). Terminology as a key uncertainty in net land use and land cover change carbon flux estimates. *Earth System Dynamics*, *5*(1), 177–195. https://doi.org/10.5194/esd-5-177-2014

Pongratz, J., Reick, C. H., Raddatz, T., & Claussen, M. (2010). Biogeophysical versus biogeochemical climate response to historical anthropogenic land cover change: Climate effects of historical land cover change. *Geophysical Research Letters*, *37*(8). https://doi.org/10.1029/2010gl043010

Pongratz, J., Schwingshackl, C., Bultan, S., Obermeier, W., Havermann, F., & Guo, S. (2021). Land Use effects on climate: Current state, recent progress, and Emerging Topics. *Current Climate Change Reports*, *7*(4), 99–120. https://doi.org/10.1007/s40641-021-00178-y

Reick, C. H., Raddatz, T., Brovkin, V., & Gayler, V. (2013). Representation of natural and anthropogenic land cover change in MPI-ESM: Land Cover in MPI-ESM. *Journal of Advances in Modeling Earth Systems*, *5*(3), 459–482. https://doi.org/10.1002/jame.20022

Schulze, E. D., Sierra, C. A., Egenolf, V., Woerdehoff, R., Irslinger, R., Baldamus, C., et al. (2020). The climate change mitigation effect of bioenergy from sustainably managed forests in Central Europe. *GCB Bioenergy*, *12*(3), 186–197. https://doi.org/10.1111/gcbb.12672

Sellar, A. A., Jones, C. G., Mulcahy, J. P., Tang, Y., Yool, A., Wiltshire, A., et al. (2019). UKESM1: Description and evaluation of the U.K. Earth system model. *Journal of Advances in Modeling Earth Systems*, *11*(12), 4513–4558. https://doi.org/10.1029/2019ms001739

Smith, H. B., Vaughan, N. E., & Forster, J. (2022). Long-term national climate strategies bet on forests and soils to reach net-zero. *Communications Earth & Environment*, *3*(1), 305. https://doi.org/10.1038/s43247-022-00636-x

Soimakallio, S., Kalliokoski, T., Lehtonen, A., & Salminen, O. (2021). On the trade-offs and synergies between forest carbon sequestration and substitution. *Mitigation and Adaptation Strategies for Global Change*, *26*(1), 4. https://doi.org/10.1007/s11027-021-09942-9

Sonntag, S., Ferrer González, M., Ilyina, T., Kracher, D., Nabel, J. E. M. S., Niemeier, U., et al. (2018). Quantifying and comparing effects of climate Engineering methods on the earth system. *Earth's Future*, *6*(2), 149–168. https://doi.org/10.1002/2017ef000620

Sonntag, S., Pongratz, J., Reick, C. H., & Schmidt, H. (2016). Reforestation in a high-CO_2 world-higher mitigation potential than expected, lower adaptation potential than hoped for: Potential of reforestation IN MPI-esm. *Geophysical Research Letters*, *43*(12), 6546–6553. https://doi.org/10.1002/2016gl068824

Swart, N. C., Cole, J. N. S., Kharin, V. V., Lazare, M., Scinocca, J. F., Gillett, N. P., et al. (2019). The Canadian earth system model version 5 (CanESM5.0.3). *Geoscientific Model Development*, *12*(11), 4823–4873. https://doi.org/10.5194/gmd-12-4823-2019

Van Vuuren, D. P., Stehfest, E., Gernaat, D. E., Doelman, J. C., Van den Berg, M., Harmsen, M., et al. (2017). Energy, land-use and greenhouse gas emissions trajectories under a green growth paradigm. *Global Environmental Change*, *42*, 237–250. https://doi.org/10.1016/j.gloenvcha.2016.05.008

Verseghy, D. L. (2000). The Canadian land surface scheme (CLASS): Its history and future. *Atmosphere-Ocean*, *38*(1), 1–13. https://doi.org/10.1080/07055900.2000.9649637

Wang, Y. P., Law, R. M., & Pak, B. (2010). A global model of carbon, nitrogen and phosphorus cycles for the terrestrial biosphere. *Biogeosciences*, *7*(7), 2261–2282. https://doi.org/10.5194/bg-7-2261-2010

Winckler, J., Lejeune, Q., Reick, C. H., & Pongratz, J. (2019). Nonlocal effects dominate the global mean surface temperature response to the biogeophysical effects of deforestation. *Geophysical Research Letters*, *46*(2), 745–755. https://doi.org/10.1029/2018gl080211

Winckler, J., Reick, C. H., Bright, R. M., & Pongratz, J. (2019). Importance of surface roughness for the local biogeophysical effects of deforestation. *Journal of Geophysical Research: Atmospheres*, *124*(15), 8605–8618. https://doi.org/10.1029/2018jd030127

Winckler, J., Reick, C. H., Luyssaert, S., Cescatti, A., Stoy, P. C., Lejeune, Q., et al. (2019). Different response of surface temperature and air temperature to deforestation in climate models. *Earth System Dynamics*, *10*(3), 473–484. https://doi.org/10.5194/esd-10-473-2019

Zhao, M., Golaz, J.-C., Held, I. M., Guo, H., Balaji, V., Benson, R., et al. (2018). The GFDL global atmosphere and land model AM4.0/LM4.0: 2. Model description, sensitivity studies, and Tuning strategies. *Journal of Advances in Modeling Earth Systems*, *10*(3), 735–769. https://doi.org/10.1002/2017ms001209

Zhu, L., Li, W., Ciais, P., He, J., Cescatti, A., Santoro, M., et al. (2023). Comparable biophysical and biogeochemical feedbacks on warming from tropical moist forest degradation. *Nature Geoscience*, *16*(3), 244–249. https://doi.org/10.1038/s41561-023-01137-y

Ziehn, T., Chamberlain, M. A., Law, R. M., Lenton, A., Bodman, R. W., Dix, M., et al. (2020). The Australian earth system model: ACCESS-ESM1.5. *Journal of Southern Hemisphere Earth Systems Science*, *70*(1), 193–214. https://doi.org/10.1071/es19035

Zomer, R. J., Trabucco, A., Verchot, L. V., & Muys, B. (2008). Land area Eligible for afforestation and reforestation within the Clean development mechanism: A global analysis of the impact of forest definition. *Mitigation and Adaptation Strategies for Global Change*, *13*(3), 219–239. https://doi.org/10.1007/s11027-007-9087-4